Progress in quantitative elemental analyses in high *P–T* fluids using synchrotron x-ray fluorescence (SXRF)

2004 J. Phys.: Condens. Matter 16 S1197

(http://iopscience.iop.org/0953-8984/16/14/031)

INSTITUTE OF PHYSICS PUBLISHING JOURNAL OF PHYSICS: CONDENSED MATTER

J. Phys.: Condens. Matter **16** (2004) S1197–S1206 PII: S0953-8984(04)74960-7

Progress in quantitative elemental analyses in high P–T fluids using synchrotron x-ray fluorescence (SXRF)

Carmen Sanchez-Valle[1,4], Isabelle Daniel[1], Isabelle Martinez[2], Alexandre Simionovici[1,3] and Bruno Reynard[1]

[1] Laboratoire de Sciences de la Terre, UMR 5570 CNRS-ENS Lyon-UCB Lyon 1, 46, Allée d'Italie, F-69364 Lyon Cedex 07, France
[2] Laboratoire de Géochimie des Isotopes Stables, Tour 54-64, IPGP-Paris VII 2, place Jussieu, 75251 Paris Cedex 05, France
[3] ID22, European Synchrotron Radiation Facility 6, rue Jules Horowitz, BP 220, F-38043 Grenoble Cedex, France

E-mail: Carmen.Sanchez@ens-lyon.fr

Received 22 January 2004
Published 26 March 2004
Online at stacks.iop.org/JPhysCM/16/S1197
DOI: 10.1088/0953-8984/16/14/031

Abstract

Two different experimental set-ups have been installed at ID22 beamline (ESRF) for synchrotron x-ray fluorescence (SXRF) analyses in diamond anvil cells (DACs). The set-ups differ from each other by the incident energy, the focusing device and the collection geometry. Analyses of standard aqueous solutions containing well-known concentrations of Sr and Rb have been performed in both experimental configurations and the detection limits (DLs) determined. The most important factors contributing to both the fluorescence intensity yield and the background have been discussed in order to determine the experimental configuration providing the lowest detection limits. The limiting factor for the analyses at very low concentrations is the background arising from the Compton and Rayleigh scattering in the diamond anvils, which have a major contribution in the collection geometry imposed by the design of the DAC. We show that slight improvements of this design enable the acquisition of the fluorescence at 150°, permitting SXRF analyses of aqueous solutions to be performed at the 40 ppm level in a standard DAC working to 10 GPa and 600 °C, at least.

1. Introduction

Aqueous fluids are exposed throughout the Earth's crust and mantle to elevated temperatures and pressures. In subduction zones, large amounts of high saline CO_2-rich aqueous fluids are released into the mantle during the dehydration of the subducting slab [1, 2]. These

[4] Author to whom any correspondence should be addressed.

fluids are involved in many geological processes such as metamorphism, arc magmatism, deep seismicity and chemical transfers between the slab and the mantle wedge [3, 4]. The extent of mass transport in subduction zones is controlled by the ability of these fluids to dissolve large amounts of minerals at elevated P and T conditions. Consequently, modelling the fluid composition and reactivity requires the knowledge of fluid–mineral equilibria at the P–T conditions relevant to subduction. Because of the experimental difficulties in studying *in situ* mineral–fluid reactions at high P and T, mineral solubilities have so far been determined mostly by analysing the resulting quenched fluids [5, 6]. However, direct determination of fluid composition in equilibrium with minerals is required in order to avoid uncontrolled fast back reactions during quenching and decompression.

Over the last decade, synchrotron x-ray fluorescence (SXRF) has been successfully applied to earth sciences issues through the analysis of ionic species in synthetic and natural fluid inclusions [7–10]. High-energy synchrotron sources as well as developments in x-ray optics allow one to obtain micrometric beamsizes with high enough flux to undertake quantitative elemental analyses in a fluid through the thick windows of a diamond anvil cell (DAC). We have recently demonstrated that Sr concentrations as low as 1000 ppm can be detected and analysed in a DAC using a forward geometry for fluorescence collection [11]. Fluorescence detection in this configuration circumvents the use of diamond anvils specially drilled to attain the optimal 90° collection geometry [12], allowing SXRF analyses to be conducted at much higher pressures.

The experimental set-up developed at the ID22 beamline (ESRF) for *in situ* high-pressure SXRF analysis has been used to follow the dissolution of strontianite ($SrCO_3$) up to 3.6 GPa and 250 °C, by monitoring the fluorescence of Sr cations in the fluid [11]. The $SrCO_3$ crystal was placed in a solution containing Rb (0.01 m $RbNO_3$), which served as an internal calibrant. For the purpose of quantitative Sr concentration measurement, the fluorescence ratio of Rb and Sr was previously calibrated in the DAC using solutions with known concentrations of these elements, in order to determine the experimental correction factor related to the difference in the fluorescence cross section of both elements at a given excitation energy. We have shown that the corrections, accounting for x-ray attenuation along the pathway to the detector and the intrinsic efficiency of the detector, cancel out in the case of two elements with close energies for emitted x-rays (14.2 and 13.4 keV for Sr and Rb, respectively).

The results of this preliminary work emphasize that SRXF is a very suitable technique for *in situ* quantification of elements in a fluid during dissolution of minerals at high P–T conditions in a DAC. Therefore, knowledge of the detection limits in a standard DAC is required to undertake the study of other mineral assemblages with lower solubilities under P and T conditions relevant to subduction zones. The development of this technique is still in progress, and the maximal capabilities have not yet been reached.

We have thus performed fluorescence analyses of solutions with various concentrations of Sr and Rb under two experimental configurations, which differ from each other by the incident energy, the x-ray focusing device and the collection geometry. The detection limits (DLs) for the SXRF analysis are determined for each experimental configuration and the factors contributing to lower the DL discussed. Finally, we show that small modifications of the DAC itself, without significant reduction of the pressure-performance of the device, allow elemental (Sr an Rb) analyses down to the 40 ppm level, allowing work up to 10 GPa and 600 °C.

2. Experimental methods

2.1. Samples

Standard aqueous solutions of known concentrations of strontium and rubidium were prepared by dissolving high purity (99.995%) strontium nitrate ($Sr(NO_3)_2$) and rubidium nitrate

Table 1. Composition of the standard solutions used in the SXRF analyses. Rb and Sr concentrations were determined by ICP-MS and ICP-AES, respectively.

Sample	Rb concentration (ppm)	Sr concentration (ppm)
Solution 1	50(3)[a]	40(2)
Solution 2	417(25)	412(24)
Solution 3	1710(103)	7010(420)
Solution 4	1818(110)	6520(391)
Solution 5	3400(204)	5020(301)
Solution 6	3880(234)	4020(241)
Solution 7	5580(335)	2600(156)
Solution 8	6600(369)	1689(101)

[a] The numbers in parentheses indicate the estimated error in the concentration (6%).

($RbNO_3$) from Aldrich® in distilled water. The composition of the solutions was analysed after preparation by inductively coupled plasma mass spectrometry (ICP-MS) and inductively coupled plasma atomic emission spectrometry (ICP-AES) for rubidium and strontium, respectively (table 1). Analytical reproducibility was better than ±6% as determined from repeated measurements of the samples.

2.2. High pressure–high temperature techniques

Experiments were conducted using membrane-type diamond anvil cells [13], equipped with two low fluorescence type Ia diamonds of 500 μm culets. High temperature conditions were achieved using an external resistive Watlow™ heater. The power input of the heater was regulated with a temperature controller (Watlow™) which keeps the temperature to the set value within ±1 °C. The actual sample temperature is determined with an accuracy of ±2 °C using a K-thermocouple, included in the heating device, and calibrated against the temperature in the sample chamber.

Sample chambers were formed by 250 μm diameter holes drilled in stainless steel foils, pre-indented to about 70 μm thickness. Gaskets were lined with a platinum ring (200 μm inner diameter hole) in order to prevent chemical reactions with the sample at elevated temperatures. The standard solutions were then loaded in the cell under a binocular microscope without transmitted light to avoid evaporation. Special care was taken to avoid contamination of the sample during the loading procedures. The pressure inside the sample chamber was determined, with an accuracy of 5%, from the calibrated shift of the R_1 fluorescence line of a ruby chip also loaded into the experimental volume [14]. Temperature effects on ruby fluorescence were corrected using the calibration proposed in [15]. Ruby fluorescence was excited and collected using a portable optical system (PRL™) installed on the beamline. Details concerning this device can be found elsewhere [11].

2.3. Synchrotron x-ray fluorescence (SXRF)

Synchrotron x-ray fluorescence analyses were performed on the undulator beamline ID22 at the European Synchrotron Radiation Facility (ESRF). The radiation was monochromatized by means of a double silicon crystal monochromator ((111) reflection). We have used two experimental set-ups with different x-ray focusing devices, tuning the energy at 18 and 23 keV, in order to maximize the flux. Monochromatic x-rays at 18 keV were focused into a spot-size of 2×5 μm^2 using an achromatic Kirkpatrick–Baez (KB) double mirror, which delivers a high flux of 5×10^{10} photons s^{-1} [16]. The fluorescence radiation of the sample was recorded in

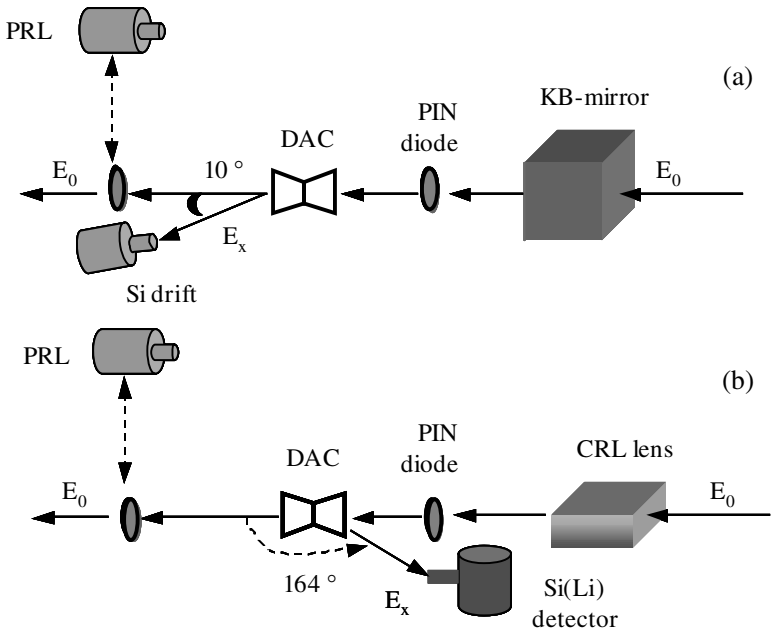

Figure 1. Schematic diagrams showing details of the experimental set-up (not to scale) installed at the ID22 beamline (ESRF) for SXRF measurements in forward transmission (a) and backscattering geometry (b), respectively.

a forward transmission geometry with a Röntec® Si drift diode detector of 8 mm^2 active area and sensitive layer thickness of 0.3 mm, positioned at 10° from the transmitted beam in the horizontal plane (figure 1(a)). At 23 keV excitation energy, the focused beam was obtained by a set of 98 parabolic aluminium compound refractive lenses (CRL) [17, 18]. This experimental set-up ensures a focal spot of 2×18 μm^2 with a flux of 5×10^9 photons s^{-1} at the sample. In this case, the emitted fluorescence was collected in backscattered geometry at 164° from the incident beam using a Eurysis® Si(Li) energy dispersive detector of 5 mm effective thickness and 150 eV resolution at 5.98 keV (figure 1(b)). In order to reduce the Compton scattering, to improve the fluorescence/scattering ratio and thereby to lower the detection limits, this detector was shielded with an Mo collimator (diameter = 4 mm), resulting in an active area of 12.5 mm^2.

The photon flux of the incident and transmitted beams were monitored using two current-integrating detectors (PIN-diodes) located before and after the sample. The DAC was mounted on the sample stage provided with one rotation and three translation motor stages. Alignment along the x-ray path was achieved by successively scanning the sample in the vertical and horizontal directions to determine the position of maximum transmission. The alignment procedures were completed with rotational scans of 5° in order to locate the DAC rotation centre, set in the focal plane of the focusing device. The cell was then rotated by 4° toward the detector in order to optimize the collection of the characteristic x-ray lines by increasing the DAC total viewing angle. The counting time for each spectrum was 1000 s. After collection, spectra were analysed using a standard peak-fitting routine (Peakfit®) in order to correct for the x-ray photon background and accurately determine the area under the characteristic x-ray fluorescence lines, assuming Voigt profiles. This area is proportional to the elemental concentration in the fluid.

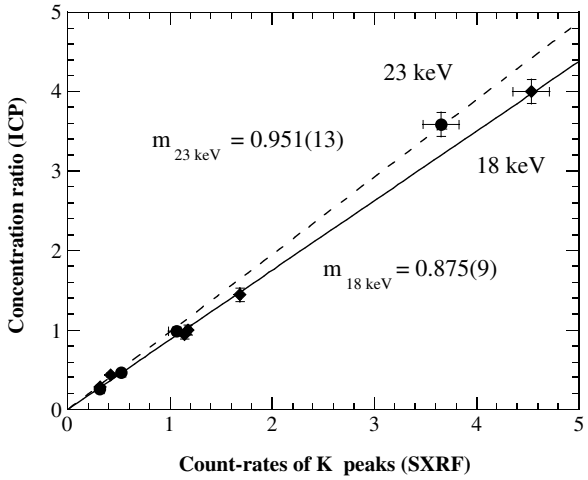

Figure 2. Plot of known concentration ratio versus measured count-rates of the Kα lines from the aqueous solution (table 1) used for fluorescence calibrations in the DAC. Diamonds: 18 keV excitation energy and 10° transmission geometry; circles: 23 keV excitation energy and 164° backscattering geometry. Solid and dashed lines, with corresponding slope values of 0.875(9) and 0.951(13), are the best fits to the data at 18 and 23 keV, respectively.

3. Results and discussion

3.1. Fluorescence calibrations in a diamond anvil cell

For Sr and Rb fluorescence calibrations, aqueous solutions containing known concentrations of both elements (table 1) were analysed in the DAC by SXRF, in both experimental configurations. The known concentration ratios determined from ICP analyses (table 1) are plotted against the count-ratio of the Kα lines obtained from SXRF analyses in figure 2. The slope of the linear correlation obtained in both set of experiments is equal, within error, to the ratio of the fluorescence cross section of Rb and Sr at the corresponding incident energies, $\sigma_F(E_0, \text{Rb})/\sigma_F(E_0, \text{Sr})$, of 0.907(45) and 0.910(42) at 18 and 23 keV, respectively [19]. The uncertainty in the experimental calibration is mainly due to the error propagation on the area of the fluorescence peaks and on the concentrations determined by ICP analysis.

The slope of the regression fit at 23 keV is closer to 1 than at 18 keV, since this excitation energy is further above the absorption edges (16.1 and 15.2 keV for Sr and Rb, respectively) and the differences in the fluorescence cross sections are reduced. The present results verify the assumption that the fluorescence yield mainly involves the fluorescence cross sections of the elements for a given incident energy [11].

In order to establish the validity of the fluorescence calibration as a function of P and T conditions, a solution containing 417 ppm of Rb and 412 ppm of Sr was analysed up to 3.20 GPa and 200 °C. The spectra collected in this solution at different P and T are displayed in figure 3. No changes in the intensity of the characteristic Kα fluorescence lines of Sr and Rb have been observed within the investigated P–T conditions. This behaviour indicates that the fluorescence cross sections are independent of P and T and also ensures that the response function of the detector for both elements is constant through a sequence of measurements. These results allow us to validate the application of the fluorescence calibration to correct the intensity ratio of Sr and Rb measured during solubility experiments at elevated P and T [11].

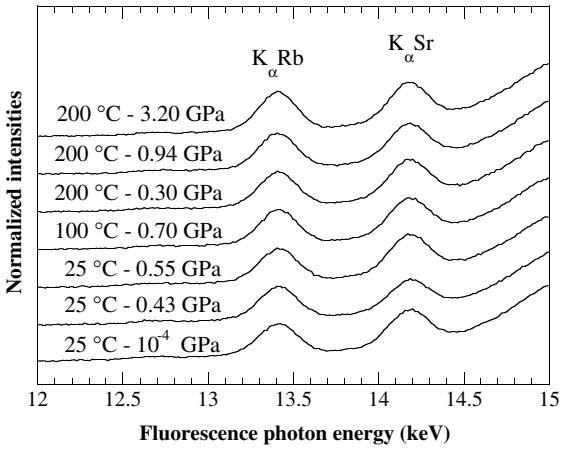

Figure 3. *In situ* SXRF recorded at different P and T conditions in a solution containing 417 ppm Rb and 412 ppm Sr. The fluorescence was excited with a 18 keV beam and collected in forward transmission geometry at 10° from the incident beam. The exposure time was 1000 s. The collected spectra were normalized by the intensity of the Compton signal. The spectra are shifted along the intensity axis for clarity.

3.2. Detection limits

The detection limits of the microprobe can be determined using standard solutions with well-known elemental compositions. Figure 4 illustrates the spectra recorded in solution 2, containing 417 ppm Rb and 412 ppm Sr (table 1), using the two experimental configurations previously described. The spectra were collected with an exposure time of 1000 s. The best counting rate obtained in figure 4(a) is associated with the highest incident flux arriving at the sample when using the Kirkpatrick–Baez mirror to focus the beam.

The concentration at the detection limit of the element i in the solution, $C_{\mathrm{DL},i}$, (in ppm), can be calculated at the 99.86% (3σ) confidence level using the following relation [20]:

$$C_{\mathrm{DL},i} = \frac{3 \times \sqrt{I_{\mathrm{B}}}}{I_i \times \sqrt{t}} \times C_i \tag{1}$$

where I_{B} and I_i are the background intensity and the net fluorescence intensity of the element i (after background subtraction) in counts per seconds, t is the acquisition time (1000 s) and C_i is the concentration of the element i in the standard solution (in ppm). From the spectra displayed in figure 4(a), using an 18 keV excitation beam of 5×10^{10} photons s^{-1} and a 10° forward transmission geometry for fluorescence collection, the DL is about 14 ppm for Rb and Sr in a solution loaded in a standard DAC. Using an incident beam of 23 keV (5×10^9 photons s^{-1}) and backscattering geometry at 164° for collection, the concentration at the DL is 43 ppm (figure 4(b)). Since measurements were performed with a similar acquisition time of 1000 s, the difference between the DL values in the two geometries is necessarily due to a difference in the peak-to-background ratio. A detailed discussion of the fluorescent emission and the different sources of scattering in both configurations is needed in order to establish the best experimental configuration, which allows one to improve the sensibility of x-ray fluorescence analyses.

At a given elemental concentration, the intensity of the characteristic fluorescence lines, I_i, depends on the illuminated sample volume (i.e., beamsize), on the fluorescence cross section of the elements at the excitation energy (E_0), and on the efficiency of the detector to collect

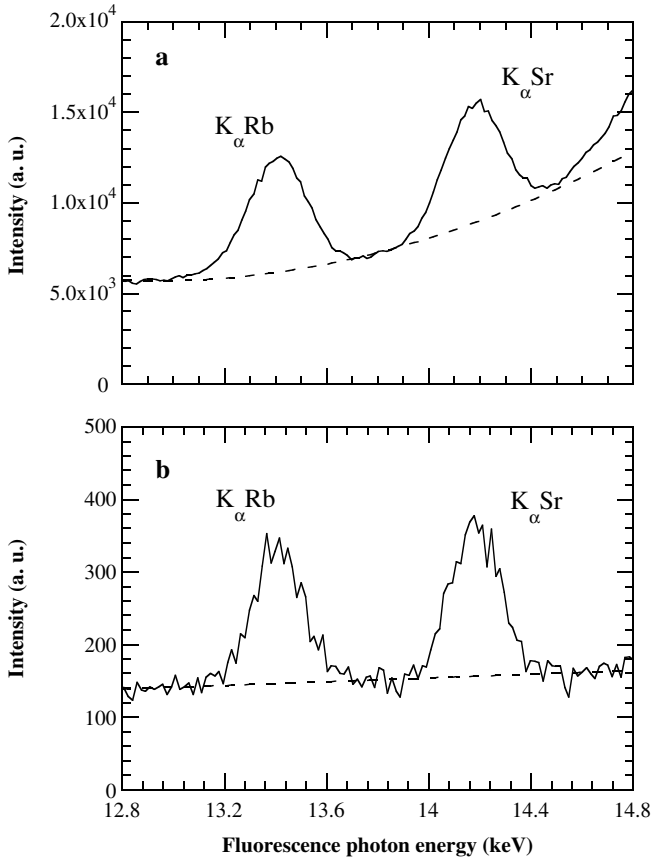

Figure 4. Comparison of fluorescence spectra recorded in a solution containing 417 ppm Rb–412 ppm Sr. (a) $E_0 = 18$ keV (5×10^{10} photons s^{-1}) and 10° transmission geometry; (b) $E_0 = 23$ keV (5×10^9 photons s^{-1}) and 164° backscattering geometry. The measurement time was 1000 s. Dashed curves: background in the region of the fluorescence lines fitted by a third-order polynomial (a) and a linear function (b).

the emitted fluorescence photons. Larger beam sizes, and hence larger excitation volumes, are obtained in the experiments using a 23 keV beam focused with the CRL lens (figure 4(b)). However, the fluorescence cross sections for the Kα lines at 18 keV for Sr and Rb are 42.68 and 38.71 cm^2 g^{-1}, whereas these values decrease respectively to 20.85 and 18.95 cm^2 g^{-1} in the case of an excitation energy of 23 keV [19]. Consequently, a more effective excitation of the illuminated sample volume is achieved using an incident beam with an energy as close as possible from the absorption edges to the elements of interest (16.1 and 15.2 keV for Sr and Rb). The optimization of the sensitivity in the experiments at 18 keV is at the origin of the lower detection limits achieved in this configuration, even when smaller excitation volumes are used and the intrinsic efficiency of fluorescence detection is lower in the case of an Si drift detector. Actually, the thicker sensitive layer of the Si(Li) detector results in almost 98% efficiency for Sr and Rb Kα lines, whereas only 60% of the these photons are counted by the Si drift detector.

Although the background has different origins, the main contribution to I_B is due to the elastic (Rayleigh) and inelastic (Compton) scattering in the diamond anvils. The contribution

of these scattered photons to the spectra, however, strongly depends on the collection geometry. The geometry is defined by the solid angle of detection (sample–detector distance, collimator diameter) and the angle of collection [21]. The solid angle of detection controls the number of fluorescence photons impinging on the detector, and thus needs to be optimized in order to improve the fluorescence/scattering ratio and to lower the detection limits. In our experiments, the solid angle subtended for the detectors was optimized by using an appropriate combination of collimator apertures and sample–detector distances, to obtain fluorescence spectra collection with a detector dead time of 20%.

Since the distribution of scattered photons is angle-dependent, the angle of collection is actually the most important factor influencing the background under the fluorescence lines. The large number of Compton/Rayleigh scattered photons reaching the detector in the 10°–164° geometry of our experiments decreases the sensitivity of the measurements, and hence increases the DLs. Theoretically, the lowest DLs are obtained when the detector is oriented perpendicular to the incoming beam, within the polarization plane of the x-ray beam; that is, in the plane of the storage ring in the case of the radiation arising from an undulator source. However, this collection geometry is not accessible in a standard diamond anvil cell without significant modifications of the original design, which reduces the pressure range for SXRF analysis to about 1 GPa [13].

In order to lower the detection limits without drastically reducing the performances of the DAC, we have slightly modified the experimental set-up previously described. Measurements were conducted in the backscattering mode with energetic and focusing conditions identical to those described in figure 1(b). In the cell, the diamond at the entrance of the beam, typically 2.2 mm thick, was replaced by a 1.2 mm thick stone. Reducing the x-ray path through the diamond reduces both the scattering phenomena and the attenuation of the fluorescence lines emitted by the sample. Moreover, reducing the thickness of the diamond window significantly increases the optical aperture of the cell, allowing much higher collection angles. The fluorescence was recorded with the Si(Li) detector set at 150° from the incoming beam, which in turn impinged on the cell with an angle of 11°.

Figure 5 illustrates the spectra recorded in a solution containing 50 ppm of Rb and 40 ppm of Sr (solution 1, table 1) using the optimized set-up (a) and the 164° backscattering geometry (b). Neither Sr nor Rb peaks emerge from the background in the case of the 164° geometry, since the concentration of the solution is within the DL calculated for this configuration (DL = 43 ppm). Actually, the concentration of one element in the sample needs to be at least three times higher than the DL in order to provide spectra that can be quantified. However, a signal corresponding to Sr and Rb is clearly observed in the spectra collected at an angle of 150°. Using equation (1), the detection limit of the microprobe in the modified configuration is calculated to be 12 ppm for Rb and Sr. Consequently, the results displayed in figure 5 demonstrate that the detection limits can be lowered by a factor 3 by reducing the thickness of the diamond window placed at the side of the detector. This modification does not significantly reduce the strength of the anvil, and SXRF analysis of the fluid can be performed at pressures up to 10 GPa.

Although lower detection limits should be achieved thanks to the higher photon flux delivered by the KB mirrors, we have preferred the use of the CRL lenses since they provide several practical advantages with respect to the former device for these particular experiments. For instance, using the KB Rh-coated mirrors now installed on ID22, the excitation energy is limited to 18 keV (energy cut-off of Rh) since the supplied photon flux rapidly decreases above this energy. In the latter case, the fluorescence lines of interest (13.4 and 14.2 keV for Rb and Sr, respectively) are superimposed on the tail of the Compton line, thus requiring the use of a third-order polynomial function to fit the background (figure 4(a)). At higher excitation energies, the

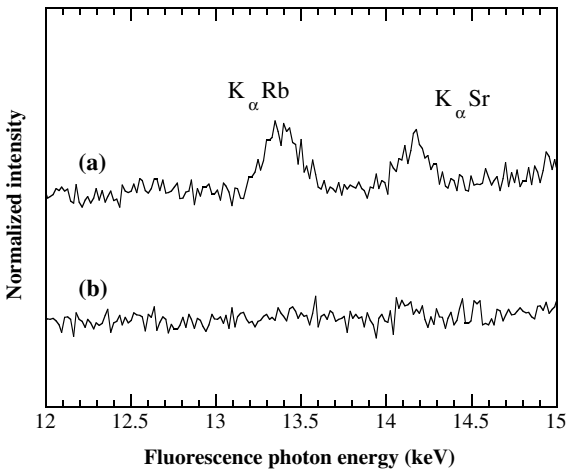

Figure 5. X-ray fluorescence spectra collected in backscattering geometry in an aqueous solution containing 50 ppm of Rb and 40 ppm of Sr: (a) 150° collection angle (1.2 mm thick diamond), (b) 164° collection angle (2.2 mm thick diamond). The spectra are shifted along the intensity axis for clarity.

background can be adjusted to a linear function (figure 4(b)), thus decreasing the uncertainties associated with the determination of the fluorescence line surfaces. In addition, the CRL in-line focusing devices with a focal distance in the range 0.5–1.5 m, allow positioning the large Si(Li) detector in backscattering geometry, whereas this configuration cannot be achieved using the KB mirrors, with only 12 cm focal distance. With the detector in the backscattering geometry, a high-resolution (1 μm) x-ray CCD camera can also be set behind the cell, in order to facilitate the alignment. Furthermore, this camera can be replaced by an imaging plate to allow simultaneous fluorescence and diffraction measurements, which are likely to be required to identify secondary mineral phases in the cell if incongruent dissolution of minerals occurs.

Acknowledgment

The authors thank C Douchet (ENS Lyon) for carrying out the ICP-MS and ICP-AES analysis of the standard solutions.

References

[1] Peacock S M 1990 *Science* **248** 329–37
[2] Scambelluri M and Philippot P 2001 *Lithos* **55** 213–27
[3] Tatsumi Y 1989 *J. Geophys. Res.* **94** 4697–707
[4] Kirby S H, Engdahl E R and Delinger R 1996 *Subduction: Top to Bottom* ed G E Bebout *et al* (Washington, DC: American Geophysical Union) pp 195–214
[5] Walther J V and Orville P M 1983 *Am. Mineral.* **68** 731–41
[6] Manning C E and Boettcher S L 1994 *Am. Mineral.* **79** 1153–8
[7] Vanko D A, Sutton S R, Riversd M L and Bodnar R J 1993 *Chem. Geol.* **109** 125–34
[8] Mavrogenes J A, Bodnar R J, Anderson A J, Bajt S, Sutton S R and Rivers M L 1995 *Geochim. Cosmochim. Acta* **59** 3987–95
[9] Philippot P, Ménez B, Chevallier P, Gibert F, Legrand F and Populus P 1998 *Chem. Geol.* **144** 121–36
[10] Ménez B, Philippot P, Bonnin-Mosbah M, Simionovici A and Gibert F 2002 *Geochim. Cosmochim. Acta* **66** 561–76

[11] Sanchez-Valle C, Martinez I, Daniel I, Philippot P, Bohic S and Simionovici A 2003 *Am. Mineral.* **88** 978–85
[12] Schmidt C and Rickers K 2003 *Am. Mineral.* **88** 288–92
[13] Chervin J C, Canny B, Besson J M and Pruzan P 1995 *Rev. Sci. Instrum.* **66** 2595–8
[14] Mao H K, Bell P M, Shaner J W and Steinber D J 1978 *J. Appl. Phys.* **49** 3276–83
[15] Ragan D R, Gustacsen R and Schiferl D 1992 *J. Appl. Phys.* **72** 5539–44
[16] Hignette O, Rostaing G, Cloetens P, Rommeveaux A, Lugwig W and Freund A 2001 X-Ray micro and nano-focusing *SPIE* **4499** 105–16
[17] Snigirev A, Kohn V G, Snigireva I and Lengeler B 1996 *Nature* **384** 49–51
[18] Lengeler B, Schroer C, Tümmler J, Benner B, Richwin M, Snigirev A, Snigireva I and Drakopoulos M 1999 *J. Synchrotron Radiat.* **6** 1153–67
[19] Brunetti A, Sanchez del Rio M, Golosio B, Simionovici A and Somogyi A 2003 *ICXOM: 17th Int. Congress on X-ray Optics and Microanalysis* p 146 (Abstracts)
[20] Helsen J A and Kuckzumow A 1993 *X-Ray Spectrometry* ed R E Van Grieken and A A Markowicz (New York: Marcel) chapter 2, p 127
[21] Somogyi A, Drakopoulos M, Vincze L, Vekemans B, Camerani C, Janssens K, Snigirev A and Adams F 2001 *X-Ray Spectrom.* **30** 242–52